Defect migration and recombination in nanoindentation of silica glass

Ken-ichi Nomura, Yi-Chun Chen, Rajiv K. Kalia, Aiichiro Nakano, and Priya Vashishta[a)]
Collaboratory for Advanced Computing and Simulations (Department of Physics and Astronomy, Department of Chemical Engineering and Materials Science, and Department of Computer Science), University of Southern California, Los Angeles, California 90089-0242, USA

Deformation, plasticity, and flow in silica-based glasses have been studied for decades, and yet important questions remain about the atomistic mechanisms underlying these processes. Our molecular dynamics simulations of nanoindentation indicate that these mechanical processes have a unified underlying atomistic mechanism. The simulations reveal that indentation nucleates under-coordinated silicon and oxygen defects, which migrate by switching bonds in string-like processes. We also observe defect annihilation in the plastic region underneath and the pileup region around the indenter. These defects have also been observed in simulations of nanovoid coalescence under hydrostatic tension and in nanovoid deformation and breakup in shearing silica glass. © *2011 American Institute of Physics*. [doi:10.1063/1.3637052]

In recent years, considerable progress has been made in indentation testing[1] by combining it with atomic force microscopy (AFM).[2–10] In indentation experiments, the hardness of a material is obtained from the ratio of the maximum applied load (P_{max}) to the contact area (A_c). Since the contact area in nanoindentation experiments is too small for direct observation by optical microscopy, one estimates the projected area (A_p) from a functional relationship between A_p and the measured contact depth (h_c). This can introduce considerable uncertainty in the value of hardness. AFM circumvents this problem by allowing direct observation of the impression created by the indenter and precise determination of the contact area.[3] Another advantage of AFM indentation tests over conventional nanoindentation is that indentation impressions can be made shallower by applying smaller normal loads in the range of nano to pico newtons. Miyake *et al.* have used AFM indentation tests to measure the hardness of fused silica and their estimate (10 GPa) is considerably lower than the one obtained by using the Oliver-Pharr relationship between the projected area and the contact depth.[3]

In the molecular dynamics (MD) simulations of nanoindentation described here, the applied load and the size of the indentation impression are comparable to those in an AFM nanoindentation experiment.[3] The MD simulation, however, has an advantage over an AFM indentation experiment in that it can provide atomistic-level stress distribution as well as the structure and dynamics of defects associated with deformation and plasticity in the system.[11–15]

Figure 1(a) shows a snapshot of one of the simulated amorphous silica (a-SiO$_2$) systems at the maximum indentation depth. This system contains 40×10^6 atoms and has dimensions 100 nm × 100 nm × 60 nm. We have also performed indentation on a system with 66×10^6 atoms in a volume of (100 nm).[3] Both amorphous systems were prepared by melting β-cristobalite and then quenching the melt incrementally to a very low temperature (see supplementary material[16]). Subsequently, periodic boundary condition in the z direction was removed and atoms within 5.5 Å from the bottom x-y plane were frozen. The two amorphous systems were heated gradually to 300 K, thermalized, and then indented normal to the x-y plane. Two kinds of indenters were used: one had a sharp tip and the other had a spherical tip of radius 10 nm. Both were rigid, square-based indenters with an apical angle of 70.5°. The indenter atoms interact with the atoms of the silica substrate via steric repulsion. The parameters of the indenter-substrate interatomic potential are given in the supplementary material.[16]

Figure 1(b) displays the applied load as a function of the penetration depth of the indenter for the amorphous system with 40×10^6 atoms. The load is calculated from the z component of the force on the indenter atoms and the area of indentation impression by dividing the system into voxels of dimension (1 nm)[3] and identifying empty voxels (without atoms) at the level of the original unperturbed surface. Upon unloading at the maximum indentation depth, the hardness values are found to be 10.6 and 12.0 GPa for the atomistically sharp and blunt indenters, respectively. These results compare favorably with the AFM measurement of hardness (10 GPa) in fused silica.[3] In the larger system (66×10^6 atoms), where the frozen atoms at the bottom of the substrate are much farther from the indenter tip, we obtain the same load-displacement curves and hardness values.

Figures 2(a) and 2(b) are snapshots of the mass density and pressure in the indented silica film at the maximum indentation depth. The density and pressure distributions around the indenter are computed from atomic distributions and virial stresses in 1 nm size voxels when the indenter is immobile. Figure 2(a) shows a considerable pileup and a 20% increase in the mass density of a-SiO$_2$ (Refs. 19 and 20) beneath the indenter relative to the mass density of bulk silica glass under ambient conditions (2.2 g/cc). Perriot *et al.* have used Raman micro-spectroscopy to characterize plastic behavior in an indentation experiment on fused silica,[21] and they find densification of up to 20%. Figure 2(b) shows a high-pressure region around the indenter and a low-pressure pile-up region where the density ranges between 1.8 and 2.0 g/cc. The maximum pressure around the indenter is 7 GPa, which is well below the critical pressure (>10 GPa) for the

a)Electronic mail: priyav@usc.edu.
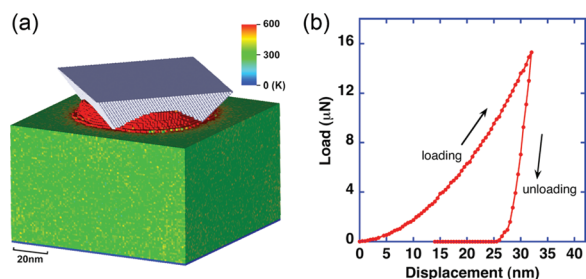
99, 111906-1

FIG. 1. (Color) (a) Pileup around the indenter at the maximum indentation depth. The colors represent "temperature" estimated from kinetic energy of atoms. (b) Load versus displacement during loading and unloading phases of indentation.

transformation to the stishovite phase of silica.[22,23] During the unloading phase of the simulation, the silica substrate exhibits elastic recovery and the density just beneath the indenter goes back to the bulk density (2.2 g/cc), although there is still significant pileup around the indenter. It should be noted that no cracks are found upon loading or unloading the indenter, which is in agreement with a recent Vickers indentation experiment by Gross and Tomozawa.[24]

Detailed analyses of atomistic configurations and stress distributions reveal that point defects in the silica network glass play a central role in the plastic deformation and pileup observed in nanoindentation simulations. Normally, the coordinations of Si and O are 4 and 2, respectively. We observe a few 5-fold coordinated Si (Ref. [25]) and 3-fold coordinated O atoms during loading. However, these over-coordinated Si and O atoms relax to their normal coordina-
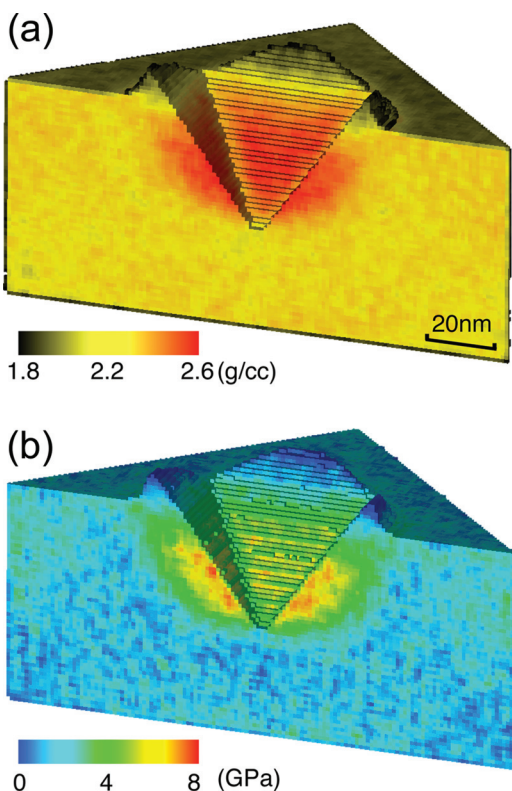
tions of 4 and 2, respectively, when the indenter is pulled out. We have also analyzed Si-O ring structure in silica glass.[26] Before indentation, the ring distribution is peaked around 6. At the maximum indentation depth, the populations of smaller rings (2, 3, and 4 fold) increase and larger rings (5, 6, 7, and 8 fold) decrease by a few percent.

The defects migrate by a bond-switching mechanism in which either a silicon or an oxygen atom severs its bond with one of its nearest neighbors and forms a new bond with a different neighbor atom. Figures 3(a)–3(c) show how such a bond-switching event occurs. The three atoms involved in this event are labeled as O1, Si2, and O3. Initially, Si2 and O3 have normal coordinations, and O1 is a non-bridging oxygen atom. At the transition state, Si2-O3 bond breaks, and these two atoms become under-coordinated. Subsequently, Si2 and O1 become fully coordinated by bonding with each other and the oxygen labeled O3 becomes a defect. Later on, O3 bonds with another Si atom that has detached from one of its oxygen neighbors.

Figures 3(d)–3(f) show the annihilation of a non-bonded pair of undercoordinated Si and O atoms. The four atoms involved in this event are labeled as Si1, O2, Si3, and O4. Initially, O2 is bonded with Si3, and they have coordinations of 2 and 4, respectively. In the transition state, O2-Si3 bond breaks, and they both become undercoordinated. In the final state, Si1 forms a bond with O2 and Si3 with O4, and now these four atoms have normal coordinations.

MD simulations reveal a mechanism of defect transport in which under-coordinated silicon and/or non-bridging oxygen atoms cascade along a chain[27] by switching bonds with their fully coordinated nearest neighbor atoms. Figure 4(a) is a snapshot of a defect migration event observed at the maximum indentation depth. Here defect migration begins when an under-coordinated silicon atom (Si1) becomes four-fold coordinated by bonding with a bridging oxygen atom (O2), and the latter severs its bond with another silicon atom (Si3). In this bond-switching process via a bridging oxygen atom, the defect migrates from the position of Si1 to the position of Si3. In the next bond-switching event, Si3 becomes fully coordinated by bonding with oxygen atom O4, and the silicon atom Si5 becomes a defect after Si5-O4 bond is broken. This bond-switching sequence terminates after silicon atom
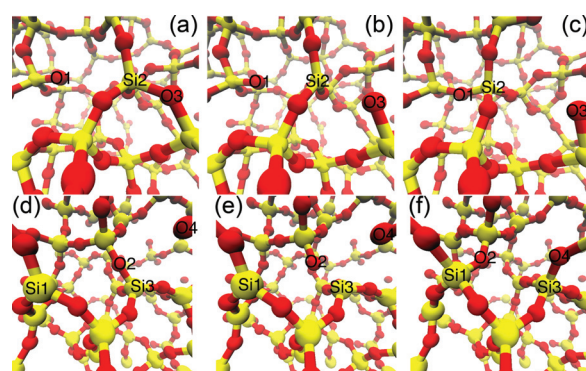

FIG. 2. (Color) (a) Density distribution and (b) pressure inside a-SiO$_2$ at the maximum load. For clarity, the panels show a diagonal cut through the substrate in the *x-y* plane. Note the densification and pressure build-up around the indenter and the low-density material pileup near the surface.

FIG. 3. (Color) (a)-(c) Snapshot showing hopping of an oxygen defect; (a) initial state, (b) transition state, and (c) final state. Atoms involved in the event are labeled as O1, Si2 and O3. The oxygen defect migrates by switching bonds from Si2-O3 to O1-Si2. Atomic configurations showing an annihilation event for a pair of defect atoms in the initial (d), transition (e), and final (f) states. Atoms involved in the event are labeled as Si1, O2, Si3 and O4.
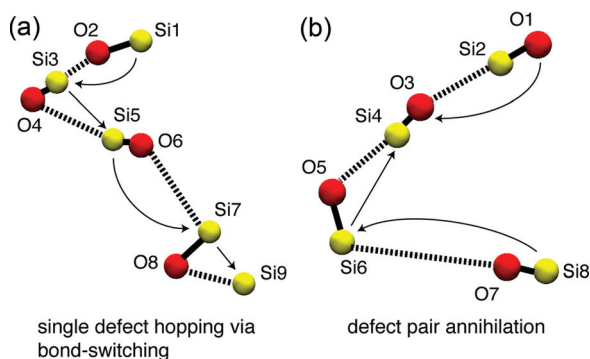
FIG. 4. (Color) Snapshots showing (a) migration of an under-coordinated Si defect and (b) annihilation of an under-coordinated Si and a non-bridging O defect. Yellow and red spheres show positions of silicon and oxygen atoms. For clarity, only the participating atoms in these events are shown. Dotted and solid lines indicate covalent bonds before and after each event. Arrows represent defect migration pathways.

Si9 becomes under-coordinated. The average speed at which this point defect cascades from Si1 to Si9 is about 200 m/s.

Figure 4(b) shows another kind of event in which a defect pair migrates along a chain and is annihilated when the two atoms become nearest neighbors. Here at the top of the chain an under-coordinated oxygen atom (O1) bonds with a silicon atom (Si2) after the bond between Si2 and another oxygen atom (O3) is broken. Thus, the non-bridging oxygen defect migrates from O1 to O3. At the bottom of the chain, an under-coordinated silicon atom (Si8) forms a bond with a bridging oxygen atom (O7) when the latter breaks its bond with another silicon atom (Si6). Next, the under-coordinated silicon defect migrates from Si6 to Si4 when the former breaks, and the latter forms a bond with a bridging oxygen atom (O5). After becoming nearest neighbors, the non-bridging oxygen (O3) bonds with under-coordinated silicon (Si4), and thus the defect pair is annihilated. The simulations also reveal reverse events where an under-coordinated silicon and a non-bridging defect pair is nucleated when the bond between them breaks and then these defects migrate away from each other by switching bonds with their nearest neighbor atoms. We have calculated the statistics of defects and find that the number of defect migration events, N_{event}, decreases exponentially with an increase in the number of bond-switching atoms, l: $N_{event} \propto \exp(-l/l_0)$. The rate of bond-switching event increases with the indentation depth: for example, at indentation depths of 8 and 28 nm, the rates of bond-switching events in the longest defect migration chain are 7×10^{11} and 1.0×10^{12} s^{-1}, respectively.

We have also estimated energy barriers for defect migration and defect pair annihilation events using the nudged elastic band method.[28] The barrier heights for these events are quite close—0.61 eV for defect migration and 0.63 eV for defect annihilation. However, the energy differences between the initial and final states for these events are substantially different (-0.64 eV for defect migration and -1.84 eV for defect pair annihilation).

In conclusion, the MD simulations of nanoindentation reveal that undercoordinated silicon and non-bridging oxygen defects in the amorphous silica network cause plastic deformation and pileup around the indenter. The defects migrate preferentially along pressure gradients on the indenter faces and along shear-stress gradients normal to the indenter faces. Such defects were theoretically postulated by Mott[29] to explain shear flow in silica glass. We have also observed these defects in MD simulations of (a) shear-induced void deformation, damage, and flow in silica glass and (b) in coalescence of nanovoids and fracture in amorphous silica.[30,31] Taken together, the simulations indicate a unified atomistic defect mechanism of deformation, flow, and fracture in silica glass.

[1]W. C. Oliver and G. M. Pharr, MRS Bull. **35**(11), 897 (2010).
[2]S. Yip, *Handbook of Materials Modeling* (Springer, Dordrecht, 2005).
[3]K. Miyake, S. Fujisawa, A. Korenaga, T. Ishida, and S. Sasaki, Jpn. J. Appl. Phys. **43**, 4602 (2004).
[4]W. C. Oliver and G. M. Pharr, J. Mater. Res. **7**(6), 1564 (1992).
[5]G. M. Pharr, Mater. Sci. Eng., A **253**(1-2), 151 (1998).
[6]G. Binnig, C. F. Quate, and C. Gerber, Phys. Rev. Lett. **56**(9), 930 (1986).
[7]G. J. Germann, S. R. Cohen, G. Neubauer, G. M. Mcclelland, H. Seki, and D. Coulman, J. Appl. Phys. **73**(1), 163 (1993).
[8]C. M. Mate, Wear **168**(1-2), 17 (1993).
[9]G. Meyer and N. M. Amer, Appl. Phys. Lett. **57**(20), 2089 (1990).
[10]G. Neubauer, S. R. Cohen, G. M. Mcclelland, D. Horne, and C. M. Mate, Rev. Sci. Instrum. **61**(9), 2296 (1990).
[11]H. P. Chen, R. K. Kalia, A. Nakano, P. Vashishta, and I. Szlufarska, J. Appl. Phys. **102**(6), 063514 (2007).
[12]Y. C. Chen, K. Nomura, R. K. Kalia, A. Nakano, and P. Vashishta, Appl. Phys. Lett. **93**(17), 171908 (2008).
[13]K. Nishimura, R. K. Kalia, A. Nakano, and P. Vashishta, Appl, Phys. Lett. **92**(16), 161904 (2008).
[14]I. Szlufarska, A. Nakano, and P. Vashishta, Science **309**(5736), 911 (2005).
[15]P. Walsh, A. Omeltchenko, R. K. Kalia, A. Nakano, P. Vashishta, and S. Saini, Appl. Phys. Lett. **82**(1), 118 (2003).
[16]See supplementary material at http://dx.doi.org/10.1063/1.3637052 for the indenter-substrate potential. Silicon nitride or diamond is used as a nano-indenter tip. Since these are hard materials (Refs. 15, 17, 18), we use a rigid indenter.
[17]J. Z. Jiang, F. Kragh, D. J. Frost, K. Stahl, and H. Lindelov, J. Phys.-Conden. Matter **13**(22), L515 (2001).
[18]T. Irifune, A. Kurio, S. Sakamoto, T. Inoue, and H. Sumiya, Nature **421**(6923), 599 (2003).
[19]N. Binggeli and J. R. Chelikowsky, Nature **353**(6342), 344 (1991).
[20]B. B. Karki, M. C. Warren, L. Stixrude, G. J. Ackland, and J. Crain, Phys. Rev. B **55**(6), 3465 (1997).
[21]A. Perriot, D. Vandembroucq, E. Barthel, V. Martinez, L. Grosvalet, C. Martinet, and B. Champagnon, J. Am. Ceram. Soc. **89**(2), 596 (2006).
[22]V. Swamy, S. K. Saxena, B. Sundman, and J. Zhang, J. Geophys. Res.-Solid Earth **99**(B6), 11787 (1994).
[23]Y. Tsuchida and T. Yagi, Nature **340**(6230), 217 (1989).
[24]T. M. Gross and M. Tomozawa, J. Non-Cryst. Solids **354**(52-54), 5567 (2008).
[25]R. J. Angel, N. L. Ross, F. Seifert, and T. F. Fliervoet, Nature **384**(6608), 441 (1996).
[26]J. P. Rino, I. Ebbsjo, R. K. Kalia, A. Nakano, and P. Vashishta, Phys. Rev. B **47**(6), 3053 (1993).
[27]C. Donati, J. F. Douglas, W. Kob, S. J. Plimpton, P. H. Poole, and S. C. Glotzer, Phys. Rev. Lett. **80**(11), 2338 (1998).
[28]G. Henkelman and H. Jonsson, J. Chem. Phys. **113**(22), 9978 (2000).
[29]N. F. Mott, Philos. Mag. B **56**(2), 257 (1987).
[30]Z. Lu, K. Nomura, A. Sharma, W. Q. Wang, C. Zhang, A. Nakano, R. Kalia, P. Vashishta, E. Bouchaud, and C. Rountree, Phys. Rev. Lett. **95**(13), 135501 (2005).
[31]Y. C. Chen, Z. Lu, K. Nomura, W. Wang, R. K. Kalia, A. Nakano, and P. Vashishta, Phys. Rev. Lett. **99**(15), 155506 (2007).